Appl. Phys. B 59, 99–115 (1994)

Applied Physics B Lasers and Optics

Invited Paper

Optical Ramsey spectroscopy on laser-trapped and thermal Mg atoms

K. Sengstock, U. Sterr, J. H. Müller, V. Rieger, D. Bettermann, W. Ertmer

Institut für Angewandte Physik der Universität Bonn, Wegelerstrasse 8, D-53115 Bonn, Germany
(Fax: +49-228/73-3474)

Received 23 November 1993/Accepted 10 May 1994

Abstract. High-resolution spectroscopic measurements on the 457 nm Mg intercombination line are reported. Studies have been performed both on atoms contained in a magneto-optical trap and on atoms in a thermal beam. We present a detailed analysis of various factors influencing resolution and accuracy for both setups, including direct comparisons. With the trapped cold atoms, a stability of 8.7×10^{-13} within 20 s has been achieved together with an accuracy of 2×10^{-15}. The direct comparison shows the limited stability of the thermal beam apparatus for integration times larger than 300 s. For shorter times, the thermal beam setup is at present more stable by a factor of three, mainly because of a better signal-to-noise ratio.

PACS: 07.65.–b, 32.80.Pj, 42.50.+j

High-resolution spectroscopy has evolved into a valuable tool in many areas of modern physics. Results obtained by high-resolution spectroscopy are often complementary to those from high-energy physics experiments, as for example the test of weak interactions in parity violation experiments on atoms [1], tests of quantum electrodynamics with hydrogen [2, 3] or positronium [4], or tests of general relativity with laboratory experiments. Also, in certain types of atom interferometers utilizing light fields as beam splitters, the phase information is read out as a minute optical frequency shift [5–8]. For precise determination of optical frequencies the present caesium frequency standard already shows deficits, especially in the available short-time stability, so that the establishment of a new, optical frequency standard is another strong motivation for high-resolution spectroscopy research [9, 10].

With the advent of laser cooling and trapping techniques [11], high-resolution spectroscopy of neutral atoms has made great progress in recent years. A cold, trapped cloud of atoms constitutes an excellent spectroscopic sample of extremely narrow velocity width at or near zero mean velocity in combination with densities equal or larger than those obtainable in atomic beams. These factors help overcome the influence of the second-order Doppler effect and the limited interaction times available at thermal energies. Several laboratories have already demonstrated that impressive results can be achieved in the microwave region [12–16], and recently optical high resolution spectroscopy has been performed using laser trapped atoms [17, 18].

A successful integration of techniques from laser manipulation and high resolution spectroscopy requires the careful choice of a suitable atomic level scheme. Cooling and trapping from a thermal beam is best achieved using a fast, closed transition while for spectroscopy 'forbidden' transitions to long-lived states are ideal. Different candidates have been discussed in the literature [19], and several groups are exploring the interesting opportunities contained in the singulet and triplet states of alkaline earth elements [20–22]. The $^1S_0$ ground state is connected via a fast transition to the $^1P_1$ excited state and through a spin-forbidden transition to the metastable $^3P_1$ level. While for magnesium the cooling transition is closed, all heavier alkaline-earth elements have low-lying ^1D states, which limit accumulation times due to optical pumping. Except for beryllium, where little data is available, magnesium also offers the narrowest intercombination transition with a linewidth as low as 31 Hz [23].

To explore the possibilities offered by the Mg level scheme we have built a Magneto-Optical Trap (MOT) [24] where up to 4×10^5 atoms can be stored at temperatures as low as 3 mK. In order to take advantage of the low velocity of the atoms and the long natural life time of the metastable state, the trapped atoms are probed in situ by a time domain version of the well-known four-zone optical Ramsey method [25]. A sequence of four light pulses from a highly stable dye laser at 457 nm is applied to the trap volume while the trapping fields are turned off. Atoms not excited to the metastable state are recaptured as soon as the trapping fields are turned on again. Their fluorescence on the

strong trapping transition is detected with a photomultiplier and provides a signal that is a 'quantum-amplified' measure of the absorption of the 457 nm laser light. In our experiments the resolution has already been better than 1.5 kHz, while the accuracy is at the 1 Hz level, since most types of systematic line shifts are significantly reduced for pulsed spectroscopy on trapped atoms.

In this paper we will describe in detail all aspects of our experiment. Section 1 will give a general overview of our research. In Sect. 2 the individual experimental components will be discussed. A central part constitutes the ultrastable dye laser spectrometer; its construction and properties will be described in Sect. 2.1. Next, the trap with its efficient capturing process and particularly its dynamics in the presence of the spectroscopy light will be discussed. In parallel to the trap apparatus we are operating a four-zone optical Ramsey experiment on a thermal beam. Its setup will be briefly explained in Sect. 2.3.

The central part of this paper, Sect. 3, is formed by the presentation of our results on Ramsey resonances both on the thermal beam and the trap under various circumstances. We have performed detailed studies on the dependence of fringe width, fringe position, fringe phase and fringe periodicity on interaction zone distance, laser power, laser phase, laser beam misalignment, suppression of either recoil component, stray electromagnetic fields, and detection geometry.

The stability of our setup in the context of optical frequency standards will be discussed in Sect. 4. We have performed a measurement of the relative frequency stability of two independent Ramsey resonances yielding a stability of better than 7×10^{-13} at an integration time of 300 s. This paper will close with an indication of areas where progress is expected in the near future.

1 General overview

The transfer of Ramsey's classical method of separated oscillatory fields [26] to the optical frequency region opens a way to use the phase information of the atomic coherence for ultrahigh resolution spectroscopy in the optical domain. Bordé pointed out in 1989 [5] that an experimental configuration in which an atom interacts sequentially with two counterpropagating pairs of parallel and equidistant resonant laser beams in fact constitutes a matter-wave interferometer. This can be illustrated through a recoil diagram [27] as in Fig. 1. The excitation probability after the fourth interaction shows an oscillating dependence on the laser frequency, corresponding to the closed paths of Fig. 1. Averaging the contributions of the open paths over an atomic velocity

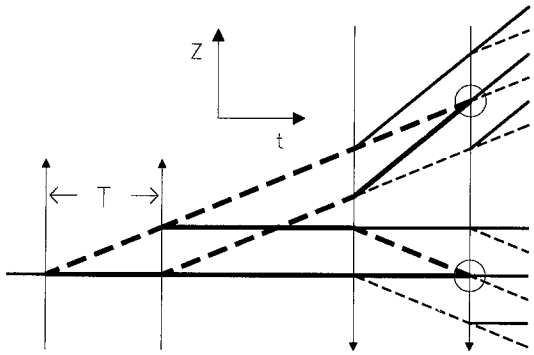

Fig. 1. Complete recoil diagram for the four-pulse Ramsey excitation. The recoil-induced separation of the atomic wave packets is shown vs time. Dashed and solid lines represent atoms traveling in the excited and ground state, respectively. The top (bottom) closed trapezoid formed by the thick lines contributes to the low- (high-) frequency recoil component of the Ramsey fringes

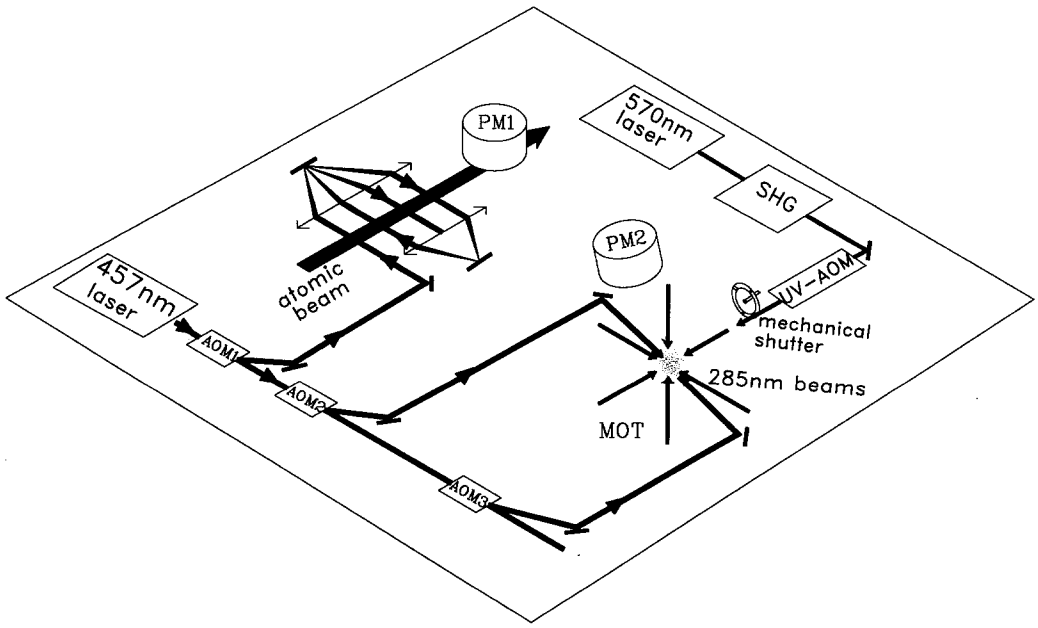

Fig. 2. Schematic view of the experimental setup for parallel spectroscopy on a thermal atomic beam and laser-cooled Mg atoms in a MOT. A detailed description is given in the text

distribution parallel to the laser beams leads to a broad background. The oscillating part can be used as a highly sensitive frequency discriminator with a resolution governed by the periodicity $1/2T$, where T denotes the time between two interaction events with laser radiation travelling in the same direction.

In our experiments we chose two different approaches to realize the described situation (Fig. 2). Laser radiation at 457 nm supplied from a high-precision dye-laser spectrometer interacts either with a Mg atomic beam by crossing it perpendicularly four times, or with a cold atomic ensemble stored in a magneto-optical trap in the form of four pulses. The pulses are produced by cutting out two pairs of light pulses of definite shape, duration and delay from two antiparallel laser beams with Acousto-optic Modulators (AOM2, AOM3, Fig. 2). These two experiments are actually run in parallel – the blue light is switched between the two setups with the aid of another modulator (AOM1) – so that a direct comparison of the performance of the two schemes can be made.

Before starting to discuss the experimental setup in detail, a reduced level scheme of the Mg atom (Fig. 3) shows the advantages but also the technical challenges one has to face in trying to reach frequency resolution well below 1 kHz with optical spectroscopy. The intercombination transition $^1S_0$–$^3P_1$ at 457 nm with an upper level lifetime of 5.1 ms [23] offers a superb frequency reference, insensitive to perturbations from external fields to a high degree. Also the fine structure transition $^3P_1$–$^3P_0$ has been discussed as a good candidate for a sub-millimeter frequency standard [28] and is now used successfully in a prototype standard at 601 GHz [29]. The resonance transition in the singlet system $^1S_0$–$^1P_1$ with an upper level lifetime of only 2.02 ns belongs to a closed two level system ideally suited for laser cooling and trapping but at a wavelength of 285 nm, where efficient solid state sources are lacking at present. Transitions from the $^3P_1$ level to higher lying states in the triplet manifold can be used for efficient detection of $^3P_1$ atoms as will be described in Sect. 2.3. Natural Mg contains a mixture of three stable isotopes ^{24,25,26}Mg. The existence

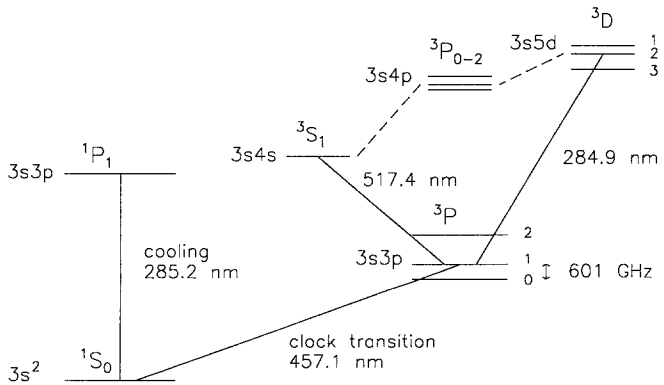

Fig. 3. Part of the Mg level scheme, showing the relevant transitions for trapping, high-resolution spectroscopy, and detection of the metastable states by laser-induced fluorescence

of both odd and even stable isotopes offers interesting experimental possibilities with regard to, e.g., laser-cooling mechanisms or quantum statistical effects in atom interferometers.

2 Experimental setup

2.1 The dye-laser spectrometer

Narrow-bandwidth 457 nm radiation is produced by a stilbene 3 dye laser, pumped by 3.5 W all-lines UV of an Ar^{++}-laser. The home-built dye laser is a compact 6 mirror design with an air-gap etalon and a birefringent filter for mode selection. Unidirectional laser operation is achieved by a Faraday polarization-rotator and a non-planar resonator layout. A piezo-mount mirror (resonance frequency of 15 kHz) and an intracavity electrooptical modulator (Gsänger PM25) act as slow and fast servo elements.

To avoid optical feedback an optical isolator is placed immediately behind the output coupler. A small part of the laser power (10 mW) is used for frequency stabilization whereas the main part is sent to the thermal atomic beam apparatus or to the magneto-optical trap.

2.1.1 The reference cavity. As the electronic servo loop locks the laser frequency to a reference cavity its stability is crucial for the whole system. All disturbances acting on the cavity lead to a broadening and shift of the laser line. The main effects are acoustic noise, temperature fluctuations (30 kHz/mK), aging of the spacer material (3 Hz/s), and air-pressure fluctuations (180 kHz/mbar), the values given for our cavity.

Our present reference cavity consists of two dielectric mirrors epoxied to a Zerodur spacer (length 518 mm, diameter 100 mm). The finesse F of this cavity was measured to be $F=800$, which corresponds to a linewidth of 400 kHz (FWHM). The mode structure is not degenerate, leading to a line profile of the cavity-resonances which is insensitive to a misalignment between the optical axis of the cavity and the laser beam. The laser beam is modematched to the TEM_{00} mode of the cavity.

The cavity is suspended in a vacuum chamber, which is evacuated to 10^{-6} mbar by an ion-getter pump. The vacuum isolates the cavity from temperature changes and prevents pressure-induced frequency shifts. The temperature of the vacuum vessel and of an inside aluminum tube are both temperature stabilized, with the inner tube held constant to 1 mK. Because of the vacuum, heat can be only transferred to the spacer by thermal radiation, which leads to a measured thermal time constant of 2.5 h between the inner shielding and the Zerodur spacer.

The Zerodur rod is suspended by two thin steel wires (diameter 0.5 mm) inside the inner aluminum tube. To reduce the coupling of mechanical disturbances to the Zerodur rod, the wires are slung around the nodes of the fundamental bending mode (at a relative distance of 0.224). The pendulum motion is damped by four Viton O-rings between the Zerodur and the aluminum-tube

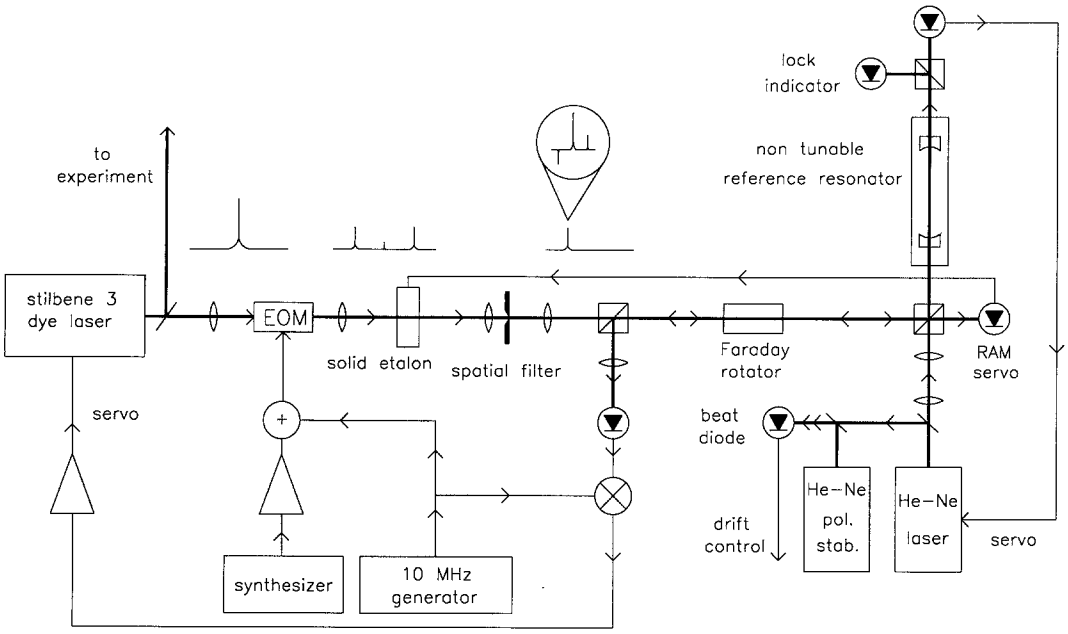

Fig. 4. Schematic setup of the dye laser spectrometer. Shown are the components for the rf-optical heterodyne stabilization scheme. The laser spectra relevant for the offset locking are indicated. Details are presented in the text. The setup shown corresponds to the 0.5–1 GHz tuning range

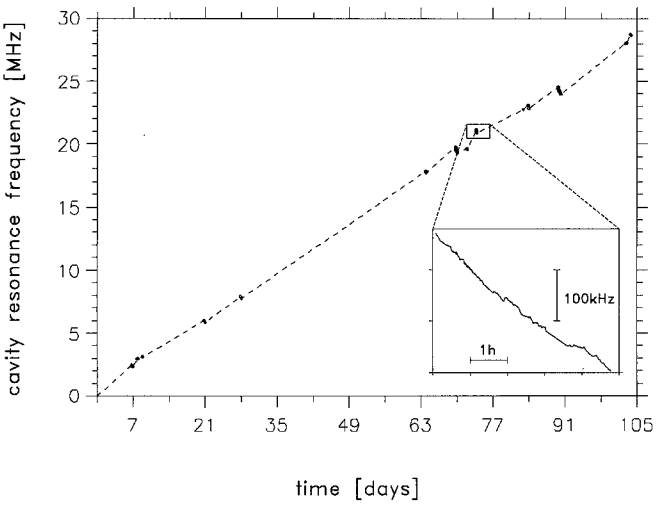

Fig. 5. Measured frequency difference (relative to an initial offset) between a single cavity mode and the Mg intercombination line vs time. The inset shows the sign reversal of the drift during an experimental run, which is probably due to a rise in ambient temperature

with a time constant of 5 s. This configuration mainly reduces horizontal acoustic noise, whereas vertical noise is only damped by the laser table (2 t concrete suspended on air buffers.)

Even with the temperature stabilized to 1 mK the cavity still slowly changes its length because of the aging of the spacer material with a rate of 3 Hz/s. This change can be monitored by a HeNe laser which is simultaneously locked to the cavity. Its frequency can be compared to a polarization stabilized HeNe laser (Fig. 4). Figure 5 shows the measured eigenfrequency of one cavity mode relative to the Mg intercombination transition. Whereas the long-term drift due to the aging of the spacer is linear, the drift during a measurement changes and even reverses its sign. This is probably because the temperature in our lab increases by up to 5 K during a measurement which leads to a small change in the temperature of the spacer. Also during the first minute after the frequency servo loop is closed a small drift of some kHz has been noticed, which we attribute to the heating of the mirrors by the light coupled into the cavity.

2.1.2 Locking scheme. The laser is locked to the cavity by a fast servo loop (Fig. 4). The error signal is generated by a frequency modulation technique, first introduced by Pound [30] in the microwave region and later adopted by Drever et al. [31] for the stabilization of laser sources. Here FM sidebands are modulated onto the laser frequency with a separation larger than the linewidth of the cavity. In the vicinity of a cavity resonance, the reflected carrier suffers a phase shift. This frequency dependent phase shift is referenced to the undisturbed reflected sidebands by heterodyning all components on a photodiode. The phase shift results in an amplitude modulation of the generated photocurrent that is synchronously demodulated with an rf mixer. A dispersion-like signal is obtained. Even for frequency fluctuations faster than the storage time of the cavity, an error signal is generated, as the internal field acts as a flywheel compared to the fluctuating incoming field.

After proportional amplification the error signal is fed to one electrode of an intracavity Electro-Optic Modulator (EOM) to provide the high-frequency servo gain. The signal is further amplified and integrated by a high-voltage operational amplifier (BB 3584) and fed to the second electrode, providing the medium-frequency range. Low-

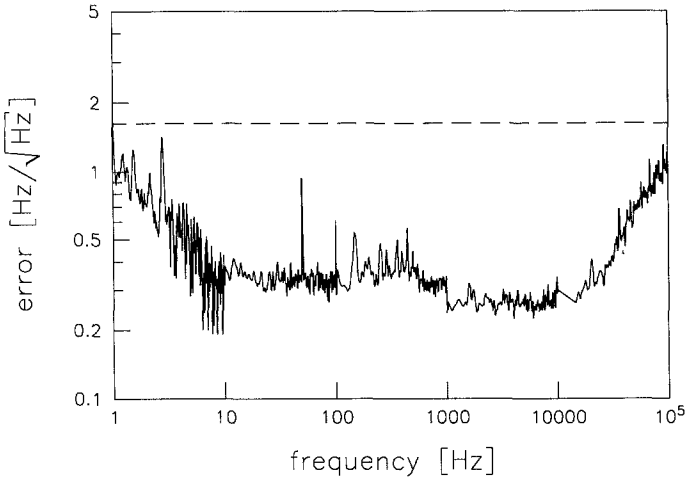

Fig. 6. Square-root of spectral-density of the laser frequency fluctuations, as derived from the electronic error signal. The dashed line indicates the shot-noise level

frequency errors are amplified and integrated once again and then fed to the piezo-driven mirror. This way the overall servo gain increases with up to 60 dB/decade towards low frequencies. As is visible in Fig. 6, the detected error signal at low frequencies is reduced even below the intrinsic noise of the frequency detector, which is mainly the shot noise of the detected photons. Actually, this shot noise introduces additional fluctuations and the spectral density of the frequency fluctuations $S_\nu(f)$ is at best limited by the shot noise, which corresponds here to $S_\nu(f) = 2.2\ \mathrm{Hz}^2/\mathrm{Hz}$. This is equivalent to a laser linewidth of 7 Hz. Note that this value is a lower limit since seismic noise on the cavity and systematic errors introduced by the locking scheme lead to larger frequency noise.

2.1.3 Systematic errors. Besides seismic noise acting on the cavity, the performance of the stabilization is limited by Residual Amplitude Modulation (RAM) introduced by the electrooptic modulator and by the etalon between the EOM and the reference cavity. This RAM leads to an offset between the cavity line center and the laser frequency, that depends on the laser power and the coupling efficiency to the cavity. To reduce this RAM a part of the laser light is picked up before it enters the cavity. It is demodulated with the same phase as the error signal. By tilting the etalon with a low voltage piezo, this signal is nulled by a servo loop. To reduce any spatial inhomogeneities a spatial filter is placed after the etalon (Fig. 4). This way the RAM has been reduced by a factor of 100.

2.1.4 Tuning. As the reference cavity is not tunable, a variable frequency offset with respect to the laser is achieved by means of optical sidebands, produced by a wideband electro-optic phase modulator (EOM in Fig. 4). A sinusoidal phase modulation with modulation index M introduces sidebands at a distance of multiples of the modulation frequency, the relative power of the n-th sideband being equal to the square of the Bessel function $J_n(M)$.

With a solid etalon (finesse 30, free spectral range 10 GHz) the lower-frequency first-order sideband is selected for the stabilization. As the optical frequency of this sideband is locked to the reference cavity, the etalon's transmission frequency does not have to be changed during a scan of the laser.

The wideband electrooptic modulator consists of a $LiTaO_3$ crystal of length 25 mm and cross section 0.5 mm × 0.65 mm in a traveling-wave configuration [32]. At 457 nm the $\lambda/2$ voltage is $V_{\lambda/2} = 52$ V. A maximum power in the first order sideband (34%) corresponds to a modulation index of $M = 1.8$, which is achieved with a microwave power of 5 W. The phasematching between microwave and light allows for an efficient modulation up to 3.7 GHz. To prevent optical damage introduced by the 457 nm radiation, the crystal is heated to 200° C. For wide-band tuning of the laser a 1 W amplifier with bandwidth 0.7–4.2 GHz was used, which produced first-order sidebands with 5–10% efficiency and which was driven by a computer-controlled synthesizer. The phase modulation for the laser lock was introduced as a phase modulation of the microwave itself. This way only the sidebands acquired the additional low-frequency stabilization sidebands, whereas the much stronger carrier remained unmodulated. With this configuration even a residual amount of the carrier that was transmitted by the etalon did not disturb the locking frequency. This setup was used to measure the isotopic shift of the Mg intercombination line with the laser locked to the same cavity mode [33].

For smaller tuning ranges a 10 W power amplifier (0.5–1 GHz) is used. It provides maximum efficiency in the generation of sidebands. In this case the low frequency modulation for the laser lock was added to the microwave by a diplexer. This method does modulate the carrier, but because its power is now low compared to the tuneable sidebands a small amount of modulated carrier transmitted by the etalon is tolerable.

2.2 Trap setup

To prepare a dense ensemble of cold atoms we use a modified version of the well known MOT [24]. The trap can be filled either from a thermal or a laser-slowed atomic beam.

The necessary UV-radiation at 285 nm is produced by frequency doubling the output of two home-built single-mode ring dye lasers at 570 nm. Each dye laser is pumped by a large frame Ar^+-laser. Typically an output power of 1.5 W from 9 W pump power is achieved. For second-harmonic generation an ADA crystal is placed in a ring configuration enhancement cavity. The cavity length is actively stabilized to match the dye laser frequency using the Hänsch-Couillaud scheme [34]. By temperature tuning the crystal to the phasematching temperature (−30° C) 30 mW UV-power is achieved routinely. We always have observed strong degradation of surface quality after stable operation for a few hours with crystals from different suppliers. With a new crystal we were

able to generate a maximum power of 50 mW. To allow both fast switching and active stabilization of the intensity both UV-beams are passed through fused-silica acousto-optic modulators.

The frequency of each dye laser is locked to the side of a transmission fringe of a tunable reference cavity with a free spectral range of 2 GHz. In order to eliminate the considerable frequency drift of these reference resonators and to allow reproducible setting of the absolute frequency, we have set up an iodine saturation spectrometer. Fortunately, the rather strong R115(20–1) absorption line of the I_2-molecule nearly coincides with half the $^1S_0$–$^1P_1$ transition frequency of the ^{24}Mg atom. The frequencies were calibrated by scanning over the hyperfine components of the I_2-line while detecting simultaneously the fluorescence induced by the second harmonic irradiating perpendicularly a Mg atomic beam (Fig. 7). We determined the position of the *s*-component of the I_2 line to be 14.5 MHz below one half of the ^{24}Mg transition frequency. Together with the tabulated position of the I_2 line [35] we evaluate $35051.272 \pm 0.006\ \mathrm{cm}^{-1}$ for the ^{24}Mg absolute transition frequency which agrees well with earlier published values [36, 37]. The use of sidebands created by an EOM in the iodine spectrometer allows precise tuning and offset locking the laser frequency with respect to the molecular transition.

One of the two independent UV-beams is used to slow a thermal atomic beam by the Zeeman tuning method [38]. The short lifetime of the $^1P_1$ state together with the large photon recoil leads to a high spontaneous force and thus a short stopping distance for the beam. This favors

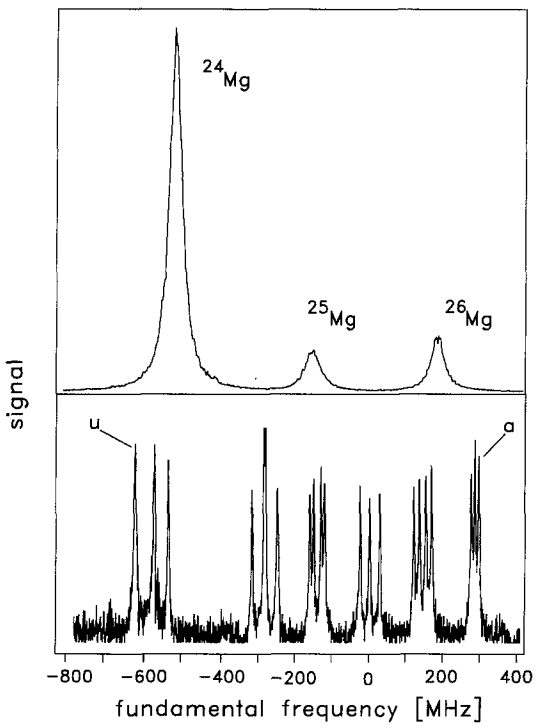

Fig. 7. Lower curve: Hyperfine structure of the *R*115 (20–1) line of I_2 obtained by saturation spectroscopy. Upper curve: Simultaneously recorded resonance fluorescence obtained by Doppler-free excitation of a Mg atomic beam with the second harmonic

the use of rare-earth permanent magnets for the slower. The longitudinal field component varies from 160 mT to −90 mT over a distance only 140 mm allowing to cover a velocity interval of 1000 m/s. The final velocity is tunable with the laser frequency from 300 m/s down to 30 m/s. The flux of cold atoms is up to 10^9 atoms/s for $v = 70$ m/s.

The MOT is situated 160 mm downstream from the end of the deceleration zone. Instead of the standard MOT setup with three independent orthogonal laser beam pairs, we decided to work with only one laser beam and a suitable configuration of mirrors and polarization optics. In this way the available UV-power is used economically, an advantage which has to be traded off against a certain amount of intensity imbalance. To avoid the accumulative transmission losses from the fused silica vacuum windows, six mirrors and a quarter-wave plate are mounted to a rigid frame inside a UHV chamber. Three of the mirrors are adjustable with piezo linear motors.

Using a trapping beam diameter of 3.4 mm we are able to store up to 4×10^5 atoms in an approximately Gaussian-shaped cloud with a diameter of 250 μm corresponding to a peak density of $10^{10}\ \mathrm{cm}^{-3}$. The measurement of the velocity distribution with a time-of-flight method yields a rms velocity below 1 m/s in accordance with standard Doppler theory for our trap parameters. Due to the large linewidth of the trapping transition the velocity capture range even for the rather small beam diameter exceeds 50 m/s. The large capture range also allows trapping from the thermal atomic beam although with three orders of magnitude less atoms in the trap. By switching between trapping from a slowed and a thermal atomic beam we are able to observe the temporal decay of the number of trapped atoms to a large alteration of the loading rate α. The decay is well described by a single exponential, thus we conclude that interaction between trapped atoms is not significant for the equilibrium number of trapped atoms. This conclusion is affirmed by the facts that we do not see a dependence of the trap diameter on the number of trapped atoms and that the fluorescence intensity from the trap for the three stable isotopes of Mg matches quite well the natural abundances. Thus the number of trapped atoms N is governed by the differential equation

$$\dot{N} = \alpha - \beta N, \tag{1}$$

with typical values for the decay constant $\beta \approx 2.5\ \mathrm{s}^{-1}$ at a background pressure below 10^{-8} mbar in our apparatus. Despite the strictly linear behavior of the trap population, the decay constant grows for increasing excitation of the atoms, a fact that is not yet fully understood and subject of current studies.

For a constant loading rate the observation of the trap fluorescence intensity, which should be exactly proportional to the trap population, allows the determination of changes in the decay constant due to additional loss mechanisms. One such loss mechanism can be the laser induced excitation to the metastable $^3P_1$ state. In this way the 'electron-shelving' effect, well known from the

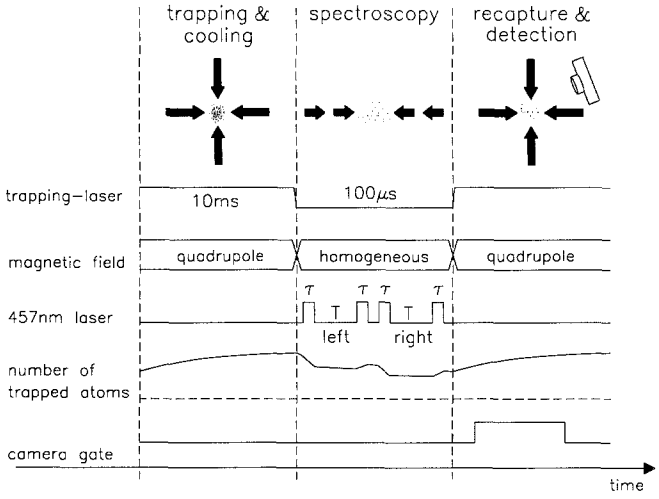

Fig. 8. Timing diagram for a spectroscopic cycle with trapped atoms. Typical values for the duration of the different sections of a cycle are indicated in the graph

spectroscopy of trapped ions [39], is used to detect a weak transition with high quantum efficiency. Furthermore, the trap dynamics in the MOT enables the action of another signal amplification due to atom 'recycling'.

A typical spectroscopic experiment cycle consists of first switching off the UV-light and switching the magnetic field from the quadrupole shape needed for trapping to a homogeneous offset field, then irradiating the freely expanding cloud of atoms with a suitable sequence of pulses from the dye laser at 457 nm and switching on the trapping fields again (Fig. 8). Atoms not excited by the blue pulses – for our experimental parameters these are more than 98% – are recaptured, compressed and velocity scrambled and thus ready to participate in the next spectroscopic cycle. In our experiments these cycles are repeated at a rate between 65 Hz and 95 Hz, so that on average an atom has more than 40 chances to jump to the $^3P_1$ level before leaving the trap for other reasons. Indeed, a straightforward but lengthy calculation shows that under the assumption of the inverse repetition rate t_C being small compared to the undisturbed trap lifetime τ_t the new equilibrium number of trapped atoms N_E is given by

$$N_E = \frac{N_0}{1 + P\tau_t/t_C}, \tag{2}$$

where P denotes the excitation probability to the $^3P_1$ level for one cycle and N_0 the number of atoms in the undisturbed trap. During our spectroscopic experiments we generally chose to work with a trap filled from the thermal atomic beam, because it tended to be more stable and the high signal amplification factor compensated for the lower initial number of atoms. The strong decrease of the whole trap fluorescence obtainable by this loss accumulation is shown in Fig. 9, where two-dimensional intensity profiles of the undisturbed trap and the trap under the action of repeated 3 μs laser pulses at 457 nm are presented.

Of course, for large amplifications the signal tends to saturate and the contrast of spectroscopic features is diminished, but the freely chooseable repetition frequency can be adjusted to optimize the signal contrast. The results obtained for Ramsey interrogation of the trapped atoms are discussed in a later section of the paper.

2.3 Setup for thermal Ramsey spectroscopy

For nonlinear Ramsey spectroscopy on a thermal beam [40] we use an interaction geometry with four running laser waves crossing perpendicularly an atomic beam [25]. The atomic beam effuses from a resistively heated furnace at 700 K. The 1 mm diameter orifice together with a pinhole of the same size placed 200 mm downstream collimates the beam to 5 mrad divergence (Fig. 10). The laser beam at 457 nm with a beam diameter of 2.4 mm and a power between 30 mW and 50 mW enters the vacuum vessel through optically flat fused-silica viewports. For retroreflection with angular deviations of less than 1 μrad achromatic lenses ($f = 400$ mm) and high reflecting mirrors in the 'cat's-eye' configura-

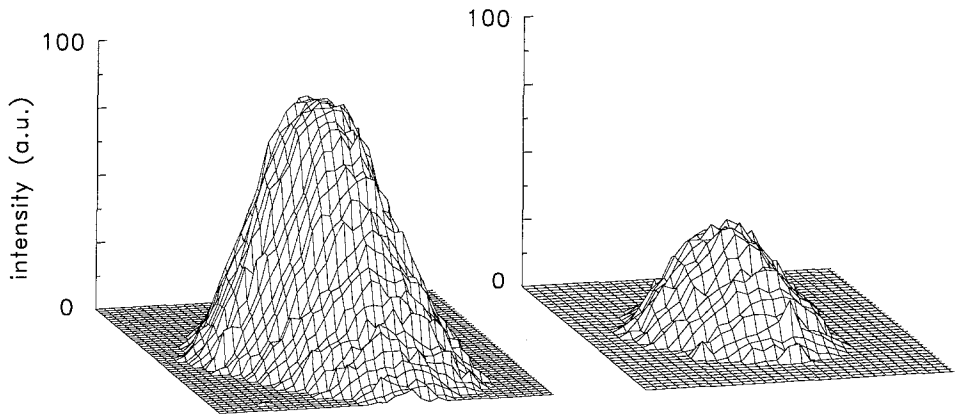

Fig. 9. Spatially resolved trap fluorescence observed with an intensified CCD camera for the undisturbed trap *(left)* and the trap under the influence of four subsequent 457 nm laser pulses of 3 μs duration applied at a rate of 90 Hz *(right)*

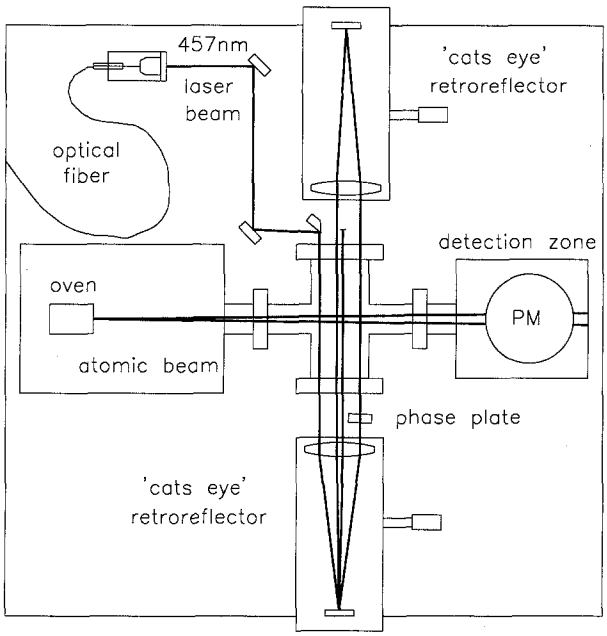

Fig. 10. Sketch of the experimental setup for Ramsey spectroscopy on a thermal beam. The optical fiber transporting the laser radiation to the apparatus is replaced for some experiments by a mirror system (see text)

tion are used [41]. The unavoidable residual spherical aberration of the lenses limits the usable range of distances of the laser beams from the optical axis for our lenses to slightly more than 22 mm. The spherical aberration can be thought of as a variation of the focal length with the distance from the optical axis. By adjusting the positions of the mirrors appropriately, it is generally possible to make three laser beams exactly parallel, but the final outgoing beam direction will remain slightly tilted against the normal. The consequences of errors of this type will be discussed together with experimental investigations in Sect. 3.

After passing the four laser interaction zones the atoms enter a separate vacuum chamber through a small hole. In this chamber the population of the excited $^3P_1$ level is probed. Due to the long lifetime of the upper level excitation and detection can be separated spatially. An excited atom at a velocity of 700 m/s travels a mean path of 3.5 m before decaying to the ground state.

Three different types of detection were tested. The most obvious choice is to detect the direct fluorescence at 457 nm. Unfortunately, the long decay length turns here into a serious drawback. Even with sophisticated light collection optics only a small fraction of the excited atoms contributes to the signal. In addition, the detection probability depends on the atomic velocity which leads to important modifications of the spectroscopic signal. Nevertheless, its simplicity and the absence of additional noise sources favor this method over the schemes described below.

A way to overcome the low efficiency of direct fluorescence detection is to selectively excite the atoms from the $^3P_1$ state to a higher lying fast decaying state in the triplet manifold (Fig. 3). We chose the $3s5d\ ^3D_2$ state with a lifetime of 34 ns and a transition wavelength of 284 nm readily accessible with our UV-laser system. The upper level decays in two main channels either directly to the $3s3p\ ^3P$ states or via a cascade involving the $3s4s\ ^3S_1$ level. The fluorescence from this level at 517 nm can be detected undisturbed by straylight from the excitation. Besides the higher detection efficiency this scheme offers the possibility to perform a sharp velocity selection by irradiating the atoms nonorthogonally to their direction of flight [42], thus allowing the detection of Ramsey fringes from a single velocity class as will be shown in Sect. 3.

The internal energy of the $^3P_1$ atoms (2.7 eV) exceeds the work function of several metals. As was first demonstrated by Lurio [43] the detection of metastable Mg by Auger electron emission from a Cs surface is feasible. In a separate experiment we prepared a Cs surface in vacuo, measured the electron emission induced by excited Mg atoms striking the surface and found detection efficiencies up to about 10%, which has to be compared with a maximum calculated efficiency of less than 0.1% for direct fluorescence detection. Problems with this method arise from the poor stability of the alkaline surface except under excellent UHV environment. In our experiment we observed intolerable drift and fluctuations in both detection efficiency and background signal from thermal electrons. For these reasons, unless otherwise noted, all spectroscopic signals from the thermal atomic beam presented in this work have been achieved by direct fluorescence detection.

3 Optical Ramsey spectroscopy

The main characteristic of the Ramsey method is a nonlinear and coherent interaction between atoms and separated light fields. From a theoretical point of view there exists a fundamental difference between the mechanical effects exerted on atoms by light fields separated in space, e.g., in thermal beam spectroscopy, and pulsed light fields separated in time. This has important consequences for interferometric applications of the Ramsey method and has been discussed in [7–8]. For the following discussion this difference is without influence, and we will attempt a common description of both spatially and temporally separated light fields. From a practical point of view there are experimental advantages unique to each method, and the following presentation is aimed to point these out in detail. We will start with a brief discussion of the signal shape, then give examples of signals obtained under various experimental conditions. Their influence on the accuracy of determining the undisturbed line center will be discussed.

3.1 Ramsey excitation

The frequency dependence of the excitation probability was calculated by Bordé et al. [44]. This calculation is performed in the atomic rest frame and therefore gives a common description of both the spatially and tempo-

rally separated excitation. The excitation probability P,

$$P = A_+(\Delta)\cos[2T(\Delta+\delta)+\Phi] + A_-(\Delta)\cos[2T(\Delta-\delta)+\Phi]+A_i(\Delta), \quad (3)$$

consists of a coherent part corresponding to the two closed trajectories of Fig. 1 plus an incoherent background $A_i(\Delta)$. The detuning $\Delta = \gamma\omega_L - \omega_0$ denotes the difference between the laser frequency ω_L and the atomic frequency ω_0 corrected for the relativistic second-order Doppler effect by the Lorentz factor $\gamma = (1-v^2/c^2)^{-1/2}$; $\delta = \hbar k^2/2m$ denotes the recoil shift, for an absolute value k of the wavevector of the laser beams and the atomic mass m. The phase Φ is the total phase difference of the four laser pulses

$$\Phi = \Phi_2 - \Phi_1 + \Phi_4 - \Phi_3 \quad (4)$$

and the factors $A_+(\Delta)$ and $A_-(\Delta)$ are weakly frequency-dependent amplitude factors taking into account the single-pulse excitation probability. While with pulsed Ramsey excitation the time T is under the control of the experimentalist and is the same for all contributing atoms, it is dependent on the atomic velocity for a beam experiment with spatially distinct interaction events. Obviously, this velocity dependence of the cosine argument in (3) can lead to a complicated signal shape $S(\omega_L)$ when averaged over the contributing ensemble.

Both for the beam and the trap experiment the detected signal can be expressed as

$$S(\omega_L) \propto \int_{v_\perp=-\infty}^{+\infty}\int_{v_\parallel=-\infty}^{+\infty} P(v_\perp, v_\parallel, \omega_L)\, N(v_\perp, v_\parallel) \times E(v_\perp, v_\parallel)\, dv_\parallel\, dv_\perp. \quad (5)$$

Here $N(v_\perp, v_\parallel)$ denotes the number of atoms of the velocity $v_\perp$ perpendicular and $v_\parallel$ parallel to the laser beams. $E(v_\perp, v_\parallel)$ is the probability for detecting an excited atom with a certain velocity. Whereas for the velocity distribution N standard expressions can be found, e.g., in [26], the dependence of the detection efficiency E on velocity is frequently neglected but can be shown to have an important influence on the detailed line shape of the Ramsey fringes.

3.2 Spectroscopic signals

We present illustrative examples of the signal in Fig. 11. The overall shape of the signal that can be observed for trapped atoms and a thermal beam consists of three parts: (*i*) the unsaturated Doppler profile of the velocity distribution in laser-beam direction with a typical width of a few MHz; (*ii*) the saturation Lamb dip whose spectral width of several hundred kHz is related to the single field interaction time; and (*iii*) the coherent part consisting of the fringe system whose periodicity is determined by the interaction time separation T. Doppler profile and Lamb dip are generated by the integration over the incoherent contributions A_i occurring in (3). In the following presentations of data they will usually be suppressed

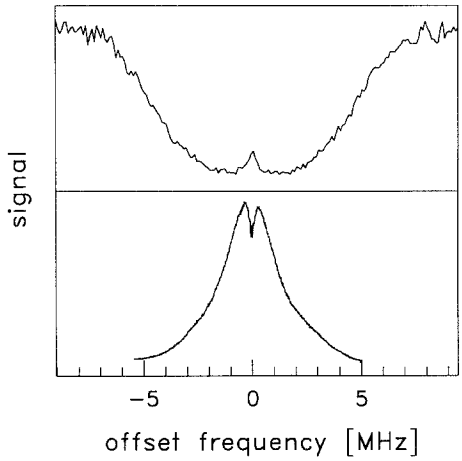

Fig. 11. Spectra of the Mg intercombination line obtained on the trap *(top)* and on the thermal atomic beam *(bottom)* showing the Doppler profile with the central Lamb dip. Because of a step-size larger than the fringe periodicity, Ramsey fringes are not visible on the upper curve

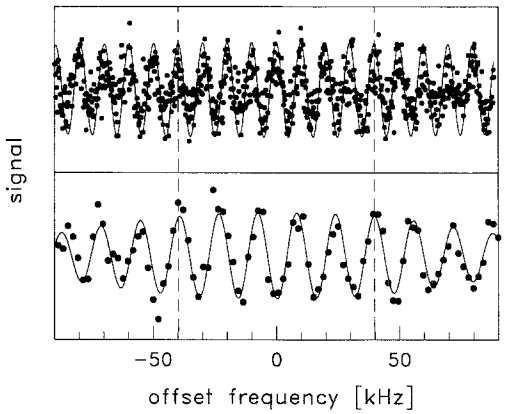

Fig. 12. Ramsey fringes on trapped atoms (top curve, pulse separation $T = 50$ μs) and on a velocity-selected atomic beam (bottom curve, velocity $v = 400$ m/s), detected by laser-induced fluorescence. The position of the recoil components is indicated by the dashed lines

by subtraction of a suitable numerical model. Asymmetries of these background terms can have a small influence on the determination of the line center of the fringe system. A convenient method to remove these residual uncertainties has been discussed by Morinaga et al. [45].

Ultimately, resolution and accuracy of the optical Ramsey method are determined from the fringe periodicity and position, respectively. For a single velocity class, the fringe position results from relativistic energy and momentum conservation and includes the atomic level separation, the photon recoil and the second-order Doppler effect (3). As usual in saturation spectroscopy, both recoil components are present, each with its own fringe system. Ramsey fringes for nearly monochromatic atomic samples are presented in Fig. 12. Since the fringe patterns cover a broader frequency interval than the recoil separation, the recoil doublet is not directly visible.

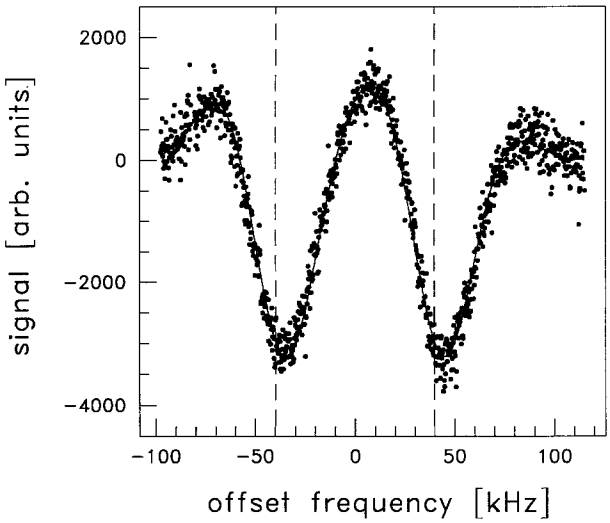

Fig. 13. Typical Ramsey fringes obtained on the thermal beam. The incoherent background consisting of Doppler profile and Lamb dip has been subtracted. The dashed lines indicate the position of the two recoil components

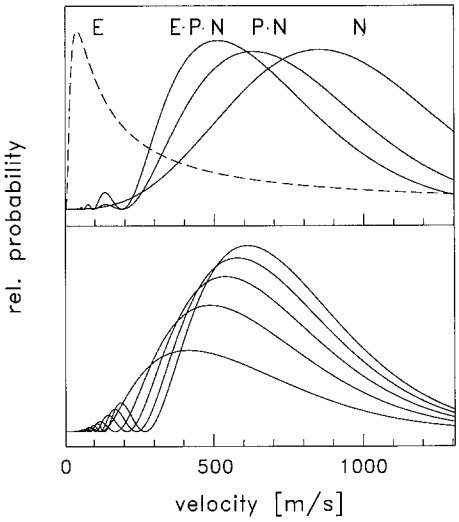

Fig. 14. Influence of the modified Maxwell-Boltzmann distribution $N(v)$, the single beam excitation probability $P(v)$, and the detection efficiency $E(v)$ on the velocity distribution of the atoms contributing to the spectroscopic signal (top curves). The values of the parameters are: temperature $T=700$ K, laser power $P=25$ mW, detector distance $s=0.2$ m, detector length $a=20$ mm. The lower curves show, from bottom to top, the velocity dependence of the total number of detected atoms for increasing laser power (10–50 mW in steps of 10 mW, all other parameters as above)

The assumption that only a single periodicity $1/2T$ contributes to the spectroscopic process, is principally satisfied for the pulsed excitation scheme. However, for thermal beam spectroscopy one has to consider the full longitudinal width of the velocity distribution N in (5). Many fringe patterns with different periodicities overlap and destructive superposition takes place. Thus only one or two fringes remain visible [26, 46]. This is illustrated in Fig. 13. The finite number of visible fringes can be attributed to a coherence length of the atomic beam. Since each velocity distribution contributes a different second-order Doppler shift, the line shape becomes asymmetric and slightly broadened. The true line center can be determined after numeric modelling following (5), correctly taking into account the contributions from all velocity classes.

3.3 Signal modeling

The three factors N, P, E of (5) show strikingly different functional dependences on $v_\perp$. The atomic velocity distribution N follows from the Maxwellian distribution and is generally described by a most probable velocity, about 750 m/s for Mg atoms at 700 K.

For the simple case of a single laser beam with rectangular intensity profile, the excitation probability $P_{\text{single beam}}$ is given by Rabi's formula

$$P_{\text{single beam}}(v_\perp) \propto \sin^2\left(\frac{\Omega w}{2v_\perp}\right). \tag{6}$$

Here Ω denotes the Rabi frequency and w the laser-beam width. Barger [46] has discussed the influence of (6) in lowest order in the Rabi frequency Ω, yielding a $v_\perp^{-2}$ dependence for the excitation probability P. The form given here is more adequate for treating Ramsey excitation where it is advantageous to work with approximately $\pi/2$ pulses [26].

For long-lived excited states, such as the $^3P_1$ metastable level ($\tau=5.1$ ms), fluorescence detection is highly velocity dependent and tends to strongly favor slow atoms: detecting over a length a a distance s behind the last excitation zone yields a detection efficiency E proportional to

$$E(v_\perp) \propto \left[1-\exp\left(-\frac{a}{v_\perp\tau}\right)\right]\exp\left(-\frac{s}{v_\perp\tau}\right). \tag{7}$$

For our typical experimental parameters such as $a=2$ cm and $s=20$ cm this results in a quite narrowly peaked function with a most probably detected velocity around 50 m/s.

We have numerically calculated the three factors N, P and E and can demonstrate their successive influence in Fig. 14. One can see that the Rabi excitation probability $P_{\text{single beam}}$ (6) modulates the velocity distribution at low velocities and that the detection probability E shifts the total distribution $E\cdot P\cdot N$ to lower velocities. The finally detected velocity distribution is strongly dependent on laser power as can been seen in the bottom part of Fig. 14. Increasing the laser power, enlarges the Rabi frequency Ω, and it follows from (6) that optimum excitation (i.e., $\pi/2$ pulses for maximum coherence) is achieved for higher velocities $v_\perp$. The oscillations at very low velocities originate from multiple Rabi floppings. For a typical laser beam width of 1.2 mm a laser power of 55 mW leads to a $\pi/2$ pulse for atoms of 500 m/s velocity. Therefore, as is visible in Fig. 14, only very slow atoms experience more than a $\pi/2$ pulse.

From the above discussion it is clear that the exact shape and position of the Ramsey signal is in an impor-

tant way influenced by the atomic velocity distribution. For high-resolution spectroscopic purposes this introduces uncertainties in the signal shape and the determination of the line center. These can either be taken into account by fitting the signal to a careful model, or fundamentally by reducing both the average velocity and the width of the velocity distribution by laser cooling. We have developed a computer code for accurate modelling of both incoherent and coherent components of the Ramsey signal. This code is able to reproduce all relevant experimental curves with only the total intensity as one free parameter. In most figures these theoretical curves are shown together with experimental data from thermal beam measurements.

3.4 Second-order Doppler effect

The influence of the second-order Doppler effect on the signal shape is most pronounced for spectra taken at large separations between the laser fields, i.e., large resolutions. We have recorded thermal beam spectra at different resolutions, which are presented in Fig. 15. One can see the second-order Doppler shift and also the increasing asymmetries of the fringes. The trapped atoms with a rms velocity of 1 m/s experience a second-order Doppler shift of less than 4 mHz, so that their spectra at different presently obtainable resolutions (Fig. 16) do not show any influence of the second-order Doppler effect. Simultaneously recorded spectra between trap and thermal beam yield a direct measurement of the second-order

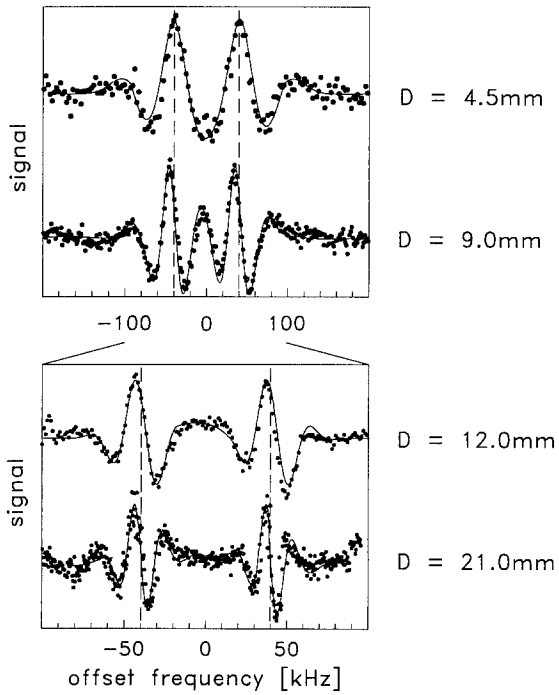

Fig. 15. Ramsey fringes on the thermal atomic beam for different resolutions. The laser beam separation D increases from top to bottom. The dashed lines indicate the position of the recoil components. Note the change in frequency scale for the lower graph

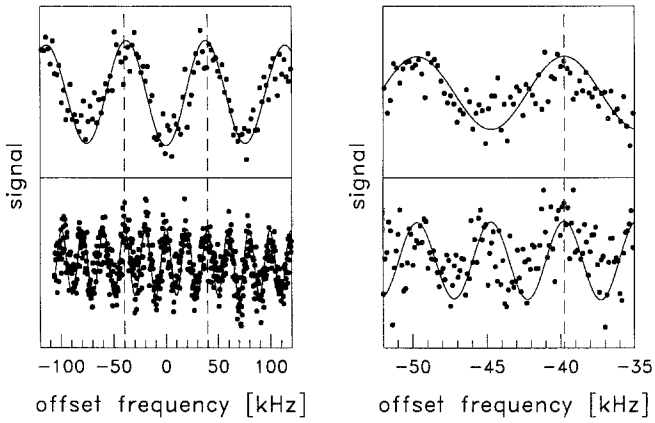

Fig. 16. Examples of Ramsey fringes of different resolutions recorded on the trap. The pulse separation time T varies from $T=6.3$ μs *(top left)*, $T=25$ μs *(bottom left)*, $T=50$ μs *(top right)* to $T=100$ μs *(bottom right)*, corresponding to a minimal periodicity of 5 kHz

Doppler shift of (-1.5 ± 0.4) kHz [17]. The error of 400 Hz results from the experimental uncertainty in determining the signal phase. From the numerical model of the signal, we can calculate an expected value of (-1.5 ± 0.3) kHz. Its error is due to an estimated 5% uncertainty in the knowledge of the contributing velocity distribution.

3.5 Power dependence

The laser power influences the Ramsey fringes through the excitation probability in two ways: as has been explained in the context of signal modeling and is visible in Fig. 14, for low powers the total number of contributing atoms decreases and the most probably contributing velocity is shifted towards lower velocities. Less participating atoms lead to a small size of the signal, while low contributing velocities result in narrower fringe width. This effect is clearly demonstrated in Fig. 17. The figure also shows, however, that the loss in contrast for low laser power is not compensated by the gain in resolution.

3.6 Phase shifts

The exact position of the fringe minimum is highly sensitive to the laser phases Φ_i, as can be seen from (3) and (4). By influencing the phase of only one of the laser beams by tilting the phase plate indicated in Fig. 10, different phases for the Ramsey fringes can be obtained. A series of such measurements is presented in Fig. 18. Optical misalignments of the cat's-eye reflector can easily cause unwanted phase differences between the laser beams and thus shift the position of the fringe minimum. For example in the scans of Fig. 17, a phase shift of approximately 60° is visible. Spectroscopy with temporally separated fields does not suffer from this problem, since the light pulses can be cut from a single beam. There

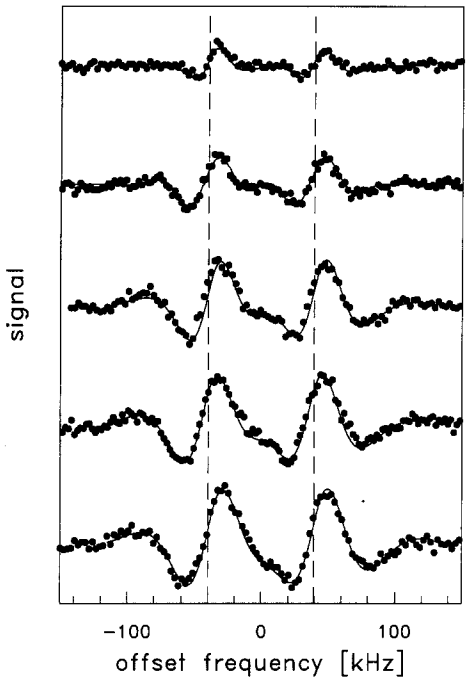

Fig. 17. Ramsey fringes obtained on the thermal beam for different laser power. The laser power varies from 10 mW (top), 20 mW, 30 mW, 40 mW to 45 mW *(bottom)*. The signal phase as deduced from the comparison with simulated signals amounts to $\Phi = 60°$

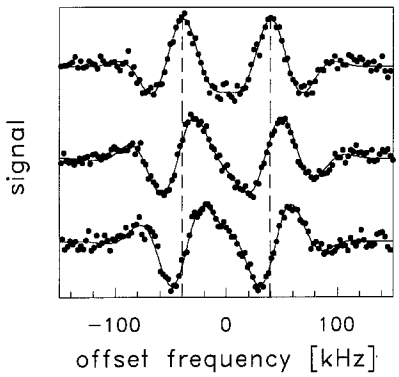

Fig. 18. Ramsey fringes obtained on the thermal beam for different laser phases Φ. The phase has been adjusted to $\Phi = 180°$, 120° and 30° *(top to bottom)*

is a minimal phase shift of the second pulse due to the heating of the AOM crystal by the first rf pulse. The temperature increase in the AOM caused by a 1 s long pulse was measured to produce a phase shift of 150 mrad. This scales down to 0.3 μrad for 2 μs long pulses used in the experiment and thus is completely negligible. There are larger phase differences conceivable between the oppositely directed pulses; however, only the difference in phase between copropagating pulses determines the phase of the Ramsey fringes. The wave vectors and the phases of the copropagating pulses are inherently the same.

3.7 Suppression of one recoil component

Another effect leading to possible systematic fringe shifts is the superposition of the two recoil components. There have been several theoretical suggestions and experimental demonstrations of different ways to eliminate either the low- or the high-frequency recoil component [8, 47–49]. We have previously demonstrated suppression of the high-frequency recoil component by introducing an UV-laser between the second and third interaction zone, thus destroying coherence for atoms that are in the ground state in this region [8]. One can also use crossover resonances between the $^3P_1(m = \pm 1)$ levels to eliminate the low-frequency recoil component [47, 50]. Examples are presented in Fig. 19.

On a thermal Mg beam it is easily possible to increase the resolution to a point where both recoil components are clearly separated in frequency so that the fringe systems do not overlap. However, the Lamb-dip backgrounds related to each component still overlap so that an exact determination of the true line center is complicated.

For pulsed Ramsey resonances on the trap both the fringe systems and the Lamb dips overlap. Line shifts due to frequency pulling of the recoil components can be reduced by choosing the fringe periodicity to be an integer fraction of the recoil separation. In this case the constructive superposition of the two fringe systems doubles the fringe contrast. For small deviations from this optimum superposition the residual pulling $\Delta\omega_P$ for the low-frequency recoil component amounts to

$$\Delta\omega_P = \delta \frac{\Delta T}{T}, \tag{8}$$

where ΔT denotes the difference between the actual pulse separation and the optimum value $T = n/4\delta$ with integer

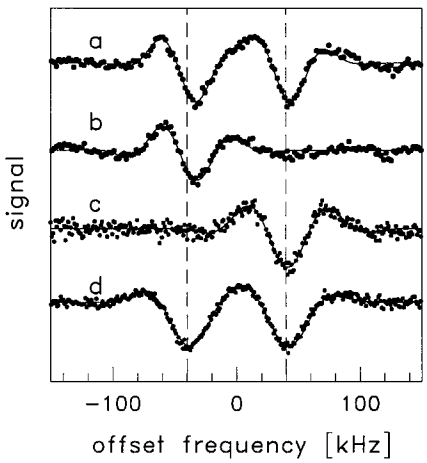

Fig. 19. Suppression of the high-frequency recoil component by an additional UV-laser beam (power, 10 mW), applied in the central dark zone. (curve *a* without, curve *b* with additional laser). Curve *c* shows Ramsey-fringes on the crossover resonance where only the high frequency recoil component is present. Curve *d* shows Ramsey fringes on the $\Delta m = 0$ transition with other experimental parameters as in *c*. All four curves have been normalized to the same amplitude

n. To reduce the pulling below 1 Hz the fractional error in pulse separation has to be below 2.5×10^{-5}. The suppression of the high-frequency recoil component, however, can be easily done by turning on the trapping laser for a few microseconds after the first pair of blue pulses.

3.8 *Optical misalignment*

One of the most critical parameter affecting precision in optical Ramsey spectroscopy is the alignment of the laser fields. Only if all four light fields are exactly parallel, the first-order Doppler effect vanishes completely. For two beams with wave vectors $\mathbf{k}_1$ and $\mathbf{k}_2$ a misalignment leads to a first-order Doppler shift $\Delta\omega_D$ of the Lamb dip

$$\Delta\omega_D = \frac{1}{2}(\mathbf{k}_1 + \mathbf{k}_2) \cdot \mathbf{v}. \tag{9}$$

For thermal atoms with velocity $v = 500$ m/s even a misalignment of 1 μrad leads to a shift of 1 kHz. On trapped, cold atoms, this shift is reduced proportional to the mean atomic velocity. In the four-zone optical Ramsey setup a similar shift and broadening of the Lamb dip is expected.

For the Ramsey fringes a misalignment leads to additional phase errors. The envelope of the Ramsey fringes will not be shifted as can be derived from the interferometric interpretation of the four-zone Ramsey setup [5, 8]. Both for beam and trap experiments the phase shift is given by the phase difference $\Phi = \Phi_2 - \Phi_1 + \Phi_4 - \Phi_3$ (4), with the phases taken at the interaction points and times. As a simple example, one can consider the case where the copropagating beams are parallel ($\mathbf{k}_1 = \mathbf{k}_2$; $\mathbf{k}_3 = \mathbf{k}_4$) but with an angular misalignment between the pairs. This leads to a phase shift $\Delta\Phi = (\mathbf{k}_1 + \mathbf{k}_3) \cdot \mathbf{v}\, T$, i.e., frequency shift $\Delta\omega = (\mathbf{k}_1 + \mathbf{k}_3) \cdot \mathbf{v}$, which is just another way of expressing the first-order Doppler shift. As indicated in Sect. 2.3, one cannot expect to achieve four exactly parallel laser beams, so that some phase errors will always remain. This phase error can be determined either by laser or atomic-beam reversal [45], or, as in our case, by comparing the signal with numerical simulations. However, even with such an analysis a remaining frequency uncertainty of 1/10 fringe width is expected.

On a thermal beam this can amount to several kHz, whereas on trapped atoms, a first-order Doppler shift will only be visible for an ensemble with a velocity distribution with non-zero mean. Otherwise angular misalignments will only lead to a reduced contrast. For the pulsed spectroscopic setup optical alignment is simpler as all interactions take place in the same region with only two laser beams involved, which allows interferometric adjustment of the beams to high precision. We have measured the velocity distribution of our trapped atoms and derive a mean velocity of less than 5% of the velocity width. Assuming a misalignment of 10 μrad, this leads to a frequency shift of 1 Hz.

Once the optical elements are well aligned, a further frequency error is introduced if the coupling of the laser light into this setup changes. This can be caused by pointing instabilities of the laser beam and environmental seismic noise. We have attempted to measure the frequency shift for the thermal setup caused by such laser beam pointing errors by deliberately misaligning our beam. We deduce a sensitivity of 2.5 kHz for 1 μrad of angular error. From the measured ambient vibrations we expect our present resolution to be limited to 3 kHz. On the trap this scales with the lower mean velocity to approximately 0.3 Hz. An optical fiber can be used to eliminate this effect, but we have also found that building vibrations disturbing the fiber lead to a frequency broadening of the laser light up to 1 kHz, caused by stress-induced index variations. We are currently testing an active stabilization scheme for the laser beam, using position-sensitive photodiodes as detectors and piezo-driven mirrors as servo-elements. Such a system combines geometrical beam stability with low power losses.

The influence of laser phase and frequency fluctuations on the Ramsey signal is discussed in more detail in the Appendix. White frequency noise leads to an exponential decrease in fringe contrast with the interaction time separation T. For example, a laser with a linewidth equal to the periodicity of the Ramsey fringes will cause the contrast to decrease to 4% of the value for strictly monochromatic light.

3.9 *Influence of external fields*

During spectroscopy the atoms fall freely because of gravity. This introduces a frequency shift, if the laser beams are not exactly horizontal. The influence of gravity on slow atoms has already been demonstrated by other authors in similar configurations [7, 51]. For perfectly aligned laser beams this shift is given by

$$\Delta\omega_g = -\frac{1}{2}(T + T_c)\,\mathbf{k}_1 \cdot \mathbf{g}, \tag{10}$$

where T_c denotes the time between the central interactions and $\mathbf{g}$ the gravitational acceleration. For a typical interaction time separation of 100 μs this corresponds to roughly 1 Hz for 1 mrad angular deviation from horizontal. Since this effect depends on the direction of the first laser beam it can be eliminated by reversing the directions of the laser beams.

On a thermal Ramsey setup the Sagnac effect also has to be taken into account and was already demonstrated by Riehle et al. [6]. Its size on the order of several Hz for the earth's rotation can affect the ultimate precision. The Sagnac effect is proportional to the oriented area enclosed by both interferometer paths. Even almost resting atoms in a trap enclose a small area during the interaction between the four pulses. This is indicated in Fig. 20. Averaging over orientations will lead to a cancellation of the individual contributions for a spherically symmetric velocity distribution. There is a slight distortion of the velocity distribution in the direction of the gravitational acceleration for trapped atoms. This will prevent exact cancellation of the individual Sagnac effects. But because of the low mean velocity the resulting magnitude of the

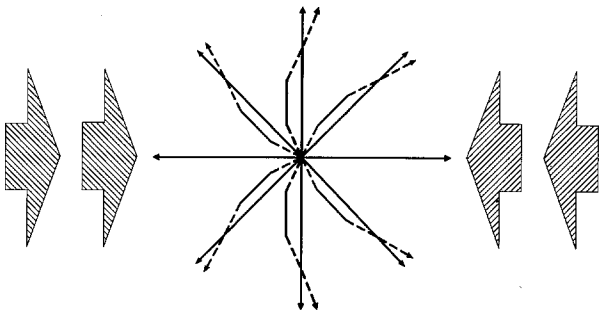

Fig. 20. Atomic trajectories corresponding to the high-frequency recoil component for an ensemble of cold atoms irradiated by two pairs of laser pulses. Because of their residual velocity atoms released from the trap move in different directions

fringe shift will be roughly 5 mHz for pulse separations of 1 ms.

Stray electromagnetic fields will also cause fringe shifts. We have measured both the ac and the dc-Stark effect for the Mg intercombination line [8, 52]. The results are well described by theoretical calculations and are presented in Fig. 21. To suppress the influence of stray electrostatic fields below 1 Hz, their size has to be reduced below 10 V/cm, which seems easily feasible. The ac-Stark shift can become significant on the trap if the extinction ratio of the shutters for the trapping light is not high enough. For a detuning of one linewidth a reduction down to 45 nW/cm^2 is necessary to keep the fringe shift to less than 1 Hz. This requires use of mechanical shutters.

3.10 Error budget

Summarizing, we have estimated the size of various effects that influence high-resolution spectroscopy on both the trap and the thermal beam. With the values given above, the total uncertainty in the determination of the true line position adds up to values of $\delta\nu_T = 500$ Hz for the thermal beam setup and of $\delta\nu_C = 1.5$ Hz for the cold-atom experiment. An overview is given in Table 1.

One effect that was not discussed is a possible pressure shift [15]. Generally, effects of binary interactions between trapped atoms have not been observed with densities as low as the ones we were using during our spectroscopic experiments ($\approx 10^7$ cm^{-3}). Therefore, we believe that for our present work pressure effects can be neglected. Nevertheless, they will become important as the density in our trap is increased. At this point it will be very interesting to study such effects with the methods of high-resolution spectroscopy.

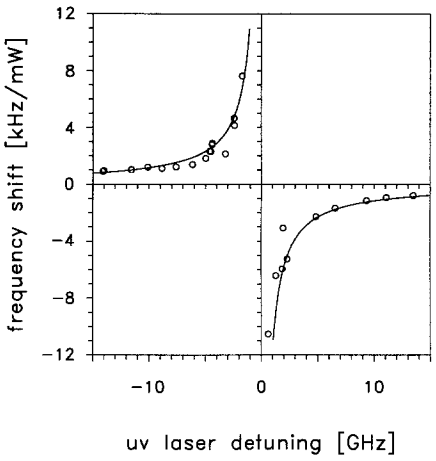

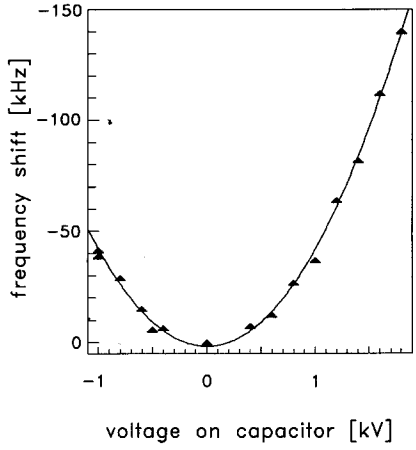

Fig. 21. Observed frequency shifts of the fringe systems dut to ac-Stark (left) and dc-Stark (right) potentials obtained on the thermal beam apparatus. For the ac-Stark case the observed shift is normalized to the UV power and shown vs the detuning of the UV laser. The solid line represents a theoretical calculation of the effect with no fit parameters. The dc-Stark shift was obtained by applying a voltage to a parallel-plate capacitor (length 5 mm, separation 1.9 mm) between the last two laser beams. This voltage is indicated in the graph. The solid line is a parabola fit to the data

Effect	Trapped atoms ($T = 3$ mK)	Thermal beam ($T = 700$ K)
Signal phase uncertainty / residual first-order Doppler effect	1 Hz	400 Hz
Uncertainty due to the second-order Doppler effect	<1 mHz	300 Hz
Asymmetric Lamb-dip background	<1 Hz	50 Hz
Wave-front curvature	<1 Hz	10 Hz
Residual electric field	<1 Hz	<1 Hz
Magnetic-field uncertainty	<1 Hz	<1 Hz
Sagnac effect	5 mHz	<1 Hz
Gravitational effect	1 Hz	1 Hz
Total uncertainty	1.5 Hz	500 Hz
$\delta\nu/\nu_0$	2×10^{-15}	7×10^{-13}

Table 1. Accuracy budget for high-resolution Ramsey spectroscopy on a thermal atomic beam and on trapped, cold atoms under conditions as discussed in the text

4 Long-term frequency stability

The precision dye-laser spectrometer, as described in Sect. 2, already has a good short-term stability that is mainly determined by the quality of the reference cavity used for optical frequency lock. Possible improvements must be of technical nature, and even though in theory conceivable, ultimately only a long-term frequency stabilization to an unperturbed narrow atomic transition will result in an excellent optical frequency reference. Several authors have previously demonstrated frequency locking of a dye laser to a central minimum of a Ramsey fringe recoil doublet obtained on a thermal beam [22, 45]. We have resolved the two recoil components in our thermal beam apparatus and stabilized our laser spectrometer to the minimum of the high-frequency recoil component. In order to obtain an independent measure of the stability and accuracy we have compared the frequency of the laser stabilized to the thermal beam resonance with the center of a Ramsey fringe obtained from the trapped atoms. The measurement yields a constant frequency offset caused mainly by the second-order Doppler effect and phase errors in the four-zone interaction geometry. More significantly, a deviation from the shot-noise-governed $\tau^{-1/2}$ behavior of the two-sample variance at integration times exceeding 300 s was observed.

Frequency stabilization was achieved by computer-controlled corrections to the offset frequency between the reference cavity and the laser carrier frequency (Sect. 2). The spectroscopic signal of both the thermal beam and the trap was measured simultaneously for roughly 0.8 s each at $+20$ kHz, 0 kHz, and -20 kHz relative to the approximate minimum of the Ramsey resonance used for stabilization. The frequency spacing for interrogation was determined by the periodicity of both signals, which was chosen to be 80 kHz on both apparatuses. The integration time at each point was taken to be long compared with the time constant of the trap dynamics, as explained in Sect. 2. After such a measurement cycle at three optical frequencies, the difference in count rates at ± 20 kHz was determined, and depending on the sign of this difference the offset frequency changed by fixed steps of ± 200 Hz. By taking small frequency corrections low servo gain was obtained and thus for short times the shot-noise-induced frequency fluctuations could be avoided. The center frequency of the trapped atoms Ramsey resonance relative to the reference cavity was determined from a parabolic fit to the count and frequency data at the three measurement points and recorded together with the actual offset frequency for later processing. By deliberately detuning the laser frequency, we have found that the parabolic fit yields a good approximation to the mainly cosine-functional dependence of the fringe shape as long as the frequency difference between the dye laser and the trapped atoms Ramsey resonance is not too large.

From the difference between the calculated center frequency of the Ramsey fringe on the MOT and the actual offset frequency we were able to compute the two-sample (Allan) variance of the frequency difference

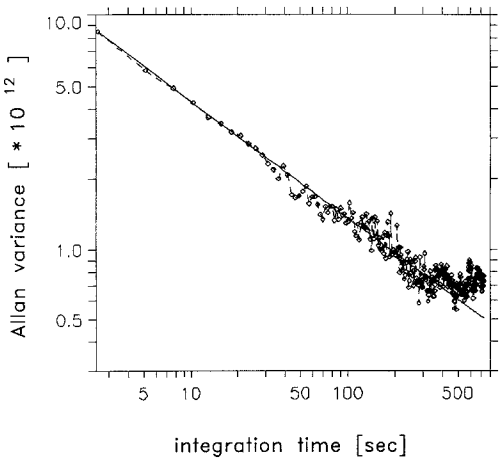

Fig. 22. Allan variance of the frequency difference between the laser stabilized to a minimum of the thermal beam Ramsey fringes and the position of a Ramsey fringe obtained on trapped, cold atoms

between the independent Ramsey resonances. The result in Fig. 22 shows a proportionality to $\tau^{-1/2}$ for integration times of less than 300 s and a distinct deviation for longer times. The linear dependence on $\tau^{-1/2}$ can be attributed to shot noise. Calculating the contributions from the trap and the thermal atomic beam we find the measured Allan variance in accordance with the value derived from the trap data and a factor of two above the thermal beam value. Since our measurement is only sensitive to the more instable of the two resonances, the data at short times therefore mainly show the shot-noise behavior of the trap. However, the flat region at large integration times must be attributed to long-term variations in the frequency of the thermal beam Ramsey resonance. Thus, our measurement yields evidence for the superiority of cold-atom optical frequency standards over their thermal counterparts. We assume that pointing instabilities and power fluctuations of the laser have caused this behavior. The long-term frequency error of 500 Hz lies within the range of the estimates given for such influences in Sect. 3.

For this experiment the fringe periodicity of both Ramsey resonances was chosen to be equal to optimize data collection. Therefore, the superior line Q that we have already achieved at the trap could not be utilized in full. With the present resolution and S/N, as shown in Fig. 16, we have already reached a shot-noise-limited fractional frequency stability of $\delta\nu/\nu \cong 1/(Q \cdot \mathrm{S/N}) = 8.7 \times 10^{-13}$ for an integration time of 20 s with trapped atoms. Similarly, if stabilization on the thermal beam were performed using fringes with resolutions as high as shown in Fig. 15, a fractional frequency stability of 3.4×10^{-13} could be achieved in 20 s.

With slightly better S/N at the trap the next logical step will be to stabilize the laser frequency to the cold atom resonance directly. This will bring a dramatic improvement in accuracy to the level of 2×10^{-15}, which cannot be obtained using the thermal beam.

5 Conclusion

We have reported detailed studies on ultrahigh-resolution spectroscopy on both laser-cooled and thermal magnesium atoms. Significant progress has been made in the integration of laser manipulation and high-resolution spectroscopy techniques. We have developed a novel way to utilize laser trapping not only for the preparation of high-quality spectroscopic samples but also for efficient detection of high-resolution signals from few neutral particles. The detection scheme employs electron shelving in the metastable triplet state and recycling of atoms that have not been excited by the narrow-linewidth laser.

Ramsey fringes on trapped, slow atoms constitute a new frequency reference which shows very small systematic line shifts and has already achieved a resolution better than previous thermal beam techniques. We have found evidence for long-term frequency errors in thermal beam Ramsey resonances. Through a detailed experimental study of the four-zone optical Ramsey setup, we have provided explanations for the causes of such behavior.

Within our present experiment several improvements should bring considerable progress in the near future. On the trap we are mainly limited by low S/N, which is governed by shot-noise fluctuations in the number of atoms. Thus, increasing the number of trapped atoms will be the next step. At this level further stabilization of the slowing, trapping and detection mechanism is necessary. To this effect, besides our present intensity- and frequency-stabilization scheme, we plan to control geometrical fluctuations in the 285 nm beams. Phase errors of the 457 nm laser beams will be minimized through an additional external optical frequency stabilizer [53] and drastically improved mechanical stability.

Future optical frequency standards will benefit greatly from the use of reliable solid-state or semiconductor lasers. While a blue-light semiconductor cw laser has already been demonstrated at room temperature [54], the only alternatives to a dye laser providing sufficient power at the 457 nm clock transition are frequency-doubled Ti:Sapphire or diode lasers [55, 56]. As high laser power is only necessary for short pulses, an intriguing possibility is the use of phase-stable pulsed amplifiers [57]. Although, the greatest challenge remains satisfactory UV generation for cooling and trapping.

An absolute frequency measurement of the Mg intercombination transition along the lines of the Munich hydrogen $1S_{1/2}$–$2S_{1/2}$ experiment [58] also seems to be feasible.

The ultimate goal for Mg optical frequency stabilization is an excitation of the extremely weak $^1S_0$–$^3P_2$ magnetic quadrupole transition. The upper state has a lifetime of more than 5500 s, i.e., a line Q of $\nu/\Delta\nu = 10^{18}$ [59].

Acknowledgements. We have greatly appreciated the experimental contributions of F. Dingler and J.v. Würzen to some of the thermal beam measurements and the helpful experimental support of F. Ruschewitz to the trap measurements. V.R. would like to acknowledge the stimulating hospitality of the Tokyo group of F. Shimizu during part of the time while this research was conducted. Financial support was provided by the Deutsche Forschungsgemeinschaft.

Appendix

Influence of finite laser linewidth on Ramsey contrast

Frequency fluctuations of the laser lead to a finite linewidth. In the case of white frequency noise ($S_\nu(f) =$ const) the corresponding phase-modulation index is inversely proportional to the Fourier frequency f. Frequencies above a certain limit will contribute less than 1 rad phase excursions, thus creating a negligible amount of sidebands. Therefore, the linewidth is proportional to S_ν. An exact calculation [60] renders a Lorentzian lineshape with a full halfwidth of

$$\nu_{1/2} = \pi S_\nu. \tag{A1}$$

Whereas the linewidth is important for linear absorption experiments, the nonlinear case requires special attention. In the case of Ramsey excitation the fringes are given by

$$P_f = C\cos\left[2\Delta T + \Phi_2(t_2) - \Phi_1(t_1) + \Phi_4(t_4) - \Phi_3(t_3)\right], \tag{A2}$$

where C describes a slowly frequency-dependent excitation probability, which will be set constant in the following. Because of the fluctuating laser frequency, the phases Φ are time dependent with mean values $\bar{\Phi}_i$ and fluctuations $\varphi_i(t)$. If we neglect changes of the optical path length between the interaction zones during the time T we are allowed to drop the index i.

Averaging over the fluctuations leads to a reduced fringe amplitude

$$\bar{P}_f = C\left\langle\cos\left(2\Delta T + \bar{\Phi}_2 - \bar{\Phi}_1 + \bar{\Phi}_4 - \bar{\Phi}_3\right) + \Delta\varphi(t)\right\rangle, \tag{A3}$$

where $\Delta\varphi(t) = \varphi(t_2) - \varphi(t_1) + \varphi(t_4) - \varphi(t_3)$ denotes the fluctuating phase difference. If we neglect the time between the second and the third interaction, which is usually much smaller than the time between the other interactions, this phase difference is given by

$$\Delta\varphi(t) = -\varphi_1(t) + \varphi_4(t + 2T). \tag{A4}$$

Using the addition theorem of the cosine, (13) can be written

$$\bar{P}_f = C\cos\left(2\Delta T + \bar{\Phi}_2 - \bar{\Phi}_1 + \bar{\Phi}_4 - \bar{\Phi}_3\right) \times\left\langle\cos\left[\varphi_1(t) - \varphi_4(t + 2T)\right]\right\rangle. \tag{A5}$$

The mean value of the fluctuation phase difference can be simplified to

$$\left\langle\cos\left(\varphi(t) - \varphi(t + 2T)\right)\right\rangle = \exp\left\{-\left\langle\left[\varphi(t) - \varphi(t + 2T)\right]^2\right\rangle/2\right\}. \tag{A6}$$

Using the relations given in [60] this is leads to

$$\left\langle\cos\left(\varphi(t) - \varphi(t + 2T)\right)\right\rangle = \exp\left[-2\int_0^\infty S_\nu(f)\,\frac{\sin^2(2\pi f T)}{f^2}\,df\right]. \tag{A7}$$

In the case of frequency fluctuations with a broadband white spectrum this leads to an exponential decrease of the coherent signal with increasing interaction time proportional to

$$\bar{P}_f \propto \exp(-2\pi^2 S_\nu T), \tag{A8}$$

or using (11):

$$\bar{P}_f \propto \exp(-2\pi\nu_{1/2} T). \tag{A9}$$

This result is directly applicable for pulsed Ramsey spectroscopy. On a thermal atomic beam the different velocity classes have to be taken into account.

References

1. M.A. Bouchiat: In *Atomic Physics 12,* ed. by J.C. Zorn, R.R. Lewis, AIP Conf. Proc. (AIP, New York 1991) p. 233
2. M. Weitz, F. Schmidt-Kahler, T.W. Hänsch: Phys. Rev. Lett. **68,** 1120 (1992)
3. F. Nez, M.D. Plimmer, S. Bourzeix, L. Julien, F. Biraben, R. Felder, O. Acef, J.J. Zondy, P. Laurent, A. Clairon, M. Abed, Y. Millerioux, P. Juncar: Phys. Rev. Lett. **69,** 2326 (1992)
4. M.S. Fee, S. Chu, A.P. Mills, R.J. Chichester, D.M. Zuckermann, E.D. Shaw, K. Danzmann: Phys. Rev. A **48,** 192 (1993)
5. C.J. Bordé: Phys. Lett. A **140,** 10 (1989)
6. F. Riehle, Th. Kisters, A. Witte, J. Helmcke, C.J. Bordé: Phys. Rev. Lett. **67,** 177 (1991)
7. M. Kasevich, S. Chu: Phys. Rev. Lett. **67,** 181 (1991)
8. U. Sterr, K. Sengstock, J.H. Müller, D. Bettermann, W. Ertmer: Appl. Phys. B **54,** 341 (1992)
9. J. Helmcke, A. Morinaga, J. Ishikawa, F. Riehle: IEEE Trans IM–**38,** 524 (1989)
10. S. Rolston, W.D. Phillips: Proc. IEEE **79,** 943 (1991)
11. For an overview see: S. Chu, C. Wieman: J. Opt. Soc. Am. B **6** (1989)
12. J.L. Hall, M. Zhu, P. Buch: J. Opt. Soc. Am. B **6,** 2194 (1989)
13. M. Kasevich, S. Chu: Phys. Rev. Lett. **63,** 612 (1989)
14. A. Clairon, C. Salomon, S. Guellati, W. Phillips: Europhys. Lett. **16,** 165 (1991)
15. K. Gibble, S. Chu: Phys. Rev. Lett. **70,** 1771 (1993)
16. M. Chowdhurry, C. Cooper, G. Hillenbrand, V. Lorent, A. Michaud, A. Steane, K. Zetie, C. Foot: In *Proc. Quantum Electronics and Laser Science Conf,* OSA Technical Digest Ser. Vol. 3 (Opt. Soc. Am., Washington, DC 1993) pp. 94–95
17. K. Sengstock, U. Sterr, G. Henning, D. Bettermann, J.H. Müller, W. Ertmer: Opt. Commun. **130,** 73 (1993)
18. Th. Kisters, K. Zeiske, F. Riehle, J. Helmcke: Verhandl. DPG (VI) **28,** 409 (1993)
19. W. Ertmer, R. Blatt, J.L. Hall: In *Laser-Cooled and Trapped Atoms,* ed. by W.D. Phillips, Natl. Bur. Stand. (U.S.) Spec. Publ., Vol. 653 (NBS, Washington, DC 1983) p. 154
20. A. Witte, Th. Kisters, F. Riehle, J. Helmcke: J. Opt. Soc. Am. B **9,** 1030 (1992)
21. T. Kurosu, M. Morinaga, F. Shimizu: Jpn. J. Appl. Phys. **31,** L273 (1992)
22. N. Ito, J. Ishikawa, A. Morinaga: J. Opt. Soc. Am. B **8,** 1388 (1991)
23. A. Godone and C. Novero: Phys. Rev. A **45,** 1717 (1992)
24. E.L. Raab, M. Prentiss, A. Cable, S. Chu, D.E. Pritchard: Phys. Rev. Lett. **59,** 2631 (1987)
25. Ch.J. Bordé, S. Avrillier, A. van Lerberghe, Ch. Salomon, D. Bassi, G. Scoles: J. Phys. (Paris) **42,** C8–15 (1981)
26. N.F. Ramsey: *Molecular Beams,* 5th edn. (Oxford Univ. Press, Oxford 1956) pp. 124–131
27. R. Beach, S.R. Hartmann, R. Friedberg: Phys. Rev. A **25,** 2658 (1982)
28. F. Strumia: Metrologia **8,** 85 (1972)
29. A. Godone, C. Novero: Metrologia **30,** 163 (1993)
30. R.V. Pound: Rev. Sci Instrum. **17,** 490 (1946)
31. R.W.P. Drever, J.L. Hall, F.V. Kowalsky, J. Hough, G.M. Ford, H. Munley, H. Ward: Appl. Phys. B **31,** 97 (1983)
32. W. Ertmer, R. Blatt, J.L. Hall, M. Zhu: Phys. Rev. Lett. **54,** 996 (1985)
33. U. Sterr, K. Sengstock, J.H. Müller, W. Ertmer: Appl. Phys. B **56,** 62 (1993)
34. T.W. Hänsch, J. Couillaud: Opt. Commun. **35,** 441 (1980)
35. S. Gerstenkorn, P. Luc: *Atlas du spectre d'absorption de la molécule de l'iode* (C.N.R.S, Paris 1978)
36. W.C. Martin, R. Zalubas: J. Phys. Chem. Ref. Data **9,** 4 (1980)
37. N. Beverini, E. Maccioni, D. Pereira, F. Strumia, G. Vissani, Y.Z. Wang: Opt. Commun. **77,** 299 (1990)
38. W.D. Phillips, H. Metcalf: Phys. Rev. Lett. **48,** 596 (1982)
39. W. Nagourney, J. Sandberg, H. Dehmelt: Phys. Rev. Lett. **56,** 2797 (1986)
40. Ye.V. Baklanov, B.Ya. Dubetski, V.P. Chebotayev: Appl. Phys. **9,** 171 (1976)
41. J.J. Snyder: Appl. Opt. **14,** 1825 (1975)
42. A. Morinaga, N. Ito, T. Sakurai: Appl. Phys. B **54,** 29 (1992)
43. A. Lurio: Phys. Rev. **126,** 1768 (1962)
44. Ch.J. Bordé, Ch. Salomon, S. Avrillier, A. Van Lerberghe, Ch. Bréant, D. Bassi, G. Scoles: Phys. Rev. A **30,** 1836 (1984)
45. A. Morinaga, F. Riehle, J. Ishikawa, J. Helmcke: Appl. Phys. B **48,** 165 (1989)
46. R.L. Barger: Opt. Lett. **6,** 145 (1981)
47. Ch.J. Bordé: In *Laser Spectroscopy III,* ed. by J.L. Hall, J.L. Carlsten, Springer Ser. Opt. Sci., Vol. 7 (Springer, Berlin, Heidelberg 1977) p. 121
48. F. Riehle, J. Ishikawa, J. Helmcke: Phys. Rev. Lett. **61,** 2092 (1988)
49. T. Kurosu, A. Morinaga: Phys. Rev. A **45,** 4799 (1992)
50. F.E. Dingler, V. Rieger, K. Sengstock, U. Sterr, W. Ertmer: Opt. Commun. (in press)
51. F. Shimizu, K. Shimizu, H. Takuma: Phys. Rev. A **46,** R17 (1992)
52. V. Rieger, K. Sengstock, U. Sterr, J.H. Müller, W. Ertmer: Opt. Commun. **99,** 172 (1993)
53. M. Zhu, J.L. Hall: J. Opt. Soc. Am. B **10,** 802 (1993)
54. N. Nakayama, S. Itoh, T. Ohata, K. Nakano, H. Okuyama, M. Ozawa, A. Ishibashi, M. Ikeda, Y. Mori: Electron. Lett. **29,** 1488 (1993)
55. S. Bourzeix, M.D. Plimmer, F. Nez, L. Julien, F. Biraben: Opt. Commun. **99,** 89 (1993)
56. W.J. Kozlovsky, W. Lenth, E.E. Latta, A. Moser, G.L. Bona: Appl. Phys. Lett. **56,** 2291 (1990)
57. M.S. Fee, K. Danzmann, S. Chu: Phys. Rev. A **45,** 4911 (1992)
58. T. Andrae, W. König, R. Wynands, D. Leibfried, F. Schmidt-Kaler, C. Zimmermann, D. Meschede, T.W. Hänsch: Phys. Rev. Lett. **69,** 1923 (1992)
59. R.H. Garstang: Astrophys. J. **148,** 579 (1967)
60. D.S. Elliott, R. Roy, S.J. Smith: Phys. Rev. A **26,** 12 (1982)